Research Article Vol. 32, No. 6 / 11 Mar 2024 / Optics Express 9297
Optics EXPRESS

Microwave coupled Zeeman splitting spectroscopy of a cesium nP_J Rydberg atom

JIABEI FAN,[1] JINGXU BAI,[1] RONG SONG,[1] YUECHUN JIAO,[1,2,*] JIANMING ZHAO,[1,2,3] AND SUOTANG JIA[1,2]

[1] State Key Laboratory of Quantum Optics and Quantum Optics Devices, Institute of Laser Spectroscopy, Shanxi University, Taiyuan 030006, China
[2] Collaborative Innovation Center of Extreme Optics, Shanxi University, Taiyuan 030006, China
[3] zhaojm@sxu.edu.cn
[*] ycjiao@sxu.edu.cn

Abstract: We perform measurements of microwave spectra of cesium Rydberg $51S_{1/2} \rightarrow 51P_J$ transitions with the linewidth approaching the Fourier limit. A two-photon scheme excites the ground-state atoms to the Rydberg $51S_{1/2}$ state, and a weak microwave photon couples the Rydberg transition of $51S_{1/2} \rightarrow 51P_J$. The hyperfine structure of $51P_{1/2}$ can be clearly resolved with a narrow linewidth microwave spectra by using the method of ion detection. Furthermore, we investigate the Zeeman effect of the $51P_{1/2,3/2}$ state. The theoretical calculations reproduce the measurement well. Our experimental measurements provide a reliable technical solution for the investigation of high angular momentum Rydberg states, which is conducive to further realizing the coherent manipulation of Rydberg energy levels and improving the sensitivity of electromagnetic field measurement.

1. Introduction

Precision spectroscopy is an important means and method to study the interaction between electromagnetic fields and matter, especially in the field of atomic and molecular physics. With the help of the inherent properties of atoms themselves and narrow linewidth microwave spectroscopy, one can explore and better understand the energy structures of atoms [1–5] and molecules [6,7], further to investigate their macroscopic and microscopic properties, physical and chemical properties [8], quantum effects [9]. Due to the unique properties like strong dipole-dipole interaction, long lifetime, large polarizability [10], Rydberg atoms have become a good candidate for investigating the interaction between laser and atom, precision spectroscopy, and quantum optics, etc. The microwave field provides a convenient way to probe and control Rydberg atoms and their interactions, as the level space between nearby Rydberg states is in the microwave range. The interaction between the microwave field and Rydberg atoms can be used to form the high-resolution narrow linewidth microwave spectroscopy in the laser cooled atoms, which has been an ideal tool to measure the level and related quantum defects of Rydberg state, especially with high angular moment l>3, which is not laser accessible [11].

The hyperfine structure of the highly excited Rydberg state is not easily observed in experiments due to its energy level space of about kHz magnitude. Fortunately, with the development of the laser and optical detecting technique, one can obtain narrow linewidth spectroscopy and access the hyperfine structure of the highly excited Rydberg state. The hyperfine structure and its coupling constant have been measured in the thermal atomic beam of Cs [12–16] and Rb [17] with low principal quantum numbers. Later, Cardman *et al*. [1] measured the hyperfine structure of $nP_{1/2}$ Rydberg states for $42 \leq n \leq 46$ using microwave spectroscopy on an ensemble of laser-cooled ^{85}Rb atoms and Li *et al*. [18] studied the $nP_{1/2}$ hyperfine structure for both ^{85}Rb and ^{87}Rb in cold Rydberg gas. Besides, Saßmannshausen *et al*. [19] observed the hyperfine structure of nS and nP Rydberg states of Cs beyond $n = 90$ in a magneto-optical trap. Meanwhile,

#515972 https://doi.org/10.1364/OE.515972
Journal © 2024 Received 13 Dec 2023; revised 17 Jan 2024; accepted 31 Jan 2024; published 29 Feb 2024

Optics EXPRESS

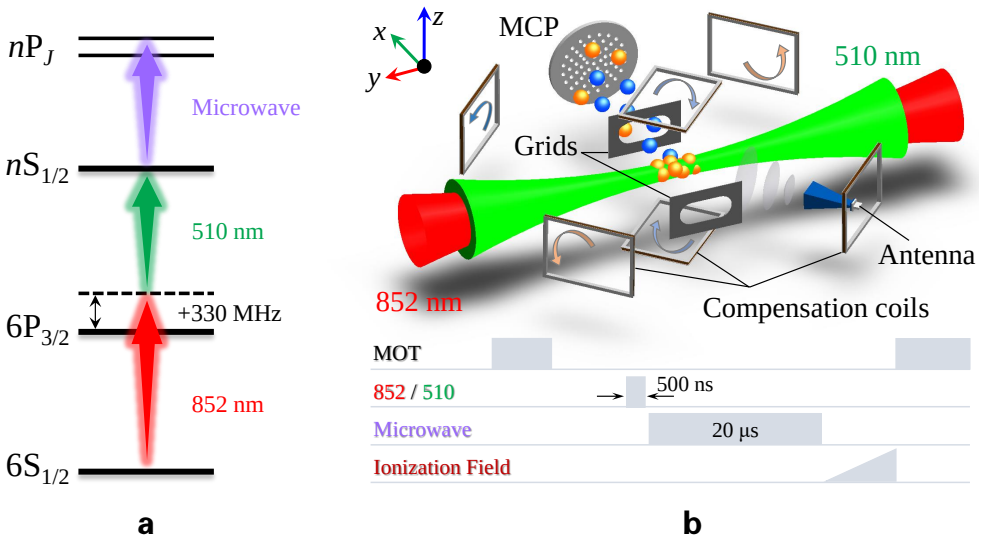

Fig. 1. (a) Overview of the level diagram of the excitation scheme. Cesium ground atoms, $6S_{1/2}(F = 4)$, are excited to $51S_{1/2}(F = 4)$ state with a two-photon (852 nm and 510 nm lasers) excitation scheme with the first photon detuning +330 MHz relative to the intermediate state, $6P_{3/2}(F' = 5)$. The microwave photon couples the neighboring Rydberg states. (b) Schematic of the experimental setup. Two excited lasers are counter-propagated through the MOT center forming the cylindrical excitation volume. Rydberg atoms are ionized with the state selective field ionization technique and collected by a micro-channel plate and processed with a boxcar connecting to a computer. Three pairs of grids (the other two pairs do not show here) and three pairs of compensation Helmholtz coils are placed on either side of the MOT which is used to compensate stray electric and magnetic fields. Microwave photons are emitted by an antenna. Schematic is not shown to scale. An experimental timing sequence is displayed in the bottom panel of (b).

rich hyperfine spectroscopy structures of Rydberg levels in a magnetic field have been studied in the room temperature cells [20–22] , as well in cold atoms [23], which has a wide range of applications in frequency stabilization [24,25], quantum information [26], Rydberg molecules [27] and Rydberg many-body dynamics [28], and Zeeman splitting of Rydberg spectroscopy is used to achieve tunable frequency measurement [29,30].

In this work, we investigate the high-resolution microwave spectra of $51S_{1/2} \rightarrow 51P_J$ transitions in cold Cs Rydberg gas by employing the two-photon excitation and microwave coupling scheme. Hyperfine structures of $51P_{1/2}$ are clearly distinguished with the spectrum linewidth near a Fourier limit. Furthermore, we obtain the precise Zeeman splittings of $51P_J$ state microwave spectroscopy in the presence of the weak magnetic field which shows a good agreement with the theoretical simulations. The precise measurement of hyperfine structure and Zeeman splittings of high-excited Rydberg state can be used to measure the magnetic field precisely.

2. Experimental setup

The experimental setup and related energy scheme are displayed in Fig. 1. Rydberg $nS_{1/2}(F = 4)$ (n=51 in this work) state are populated by a two-photon (852 nm and 510 nm lasers) excitation scheme with single photon detuning of +330 MHz. A microwave photon couples the Rydberg transition $nS_{1/2} \rightarrow nP_J$, see Fig. 1(a). Both excited lasers are external cavity diode lasers with laser frequencies locked to a 15000 high finesse Fabry-Perot cavity. The laser linewidth is less than 100 kHz. The polarization of both lasers is along with the x direction, while the polarization

Optics EXPRESS

of the microwave photon is set along the z direction, and may be changed at the atomic cloud due to the complex internal structure of the metal vacuum chamber.

Our experiment is carried out in a standard magneto-optical-trap (MOT) with a chamber vacuum pressure of 2×10^{-7} Pa. A schematic of the experiment is depicted in Fig. 1(b). 852 nm and 510 nm lasers are overlapped in a counter-propagating geometry through the MOT center, forming a cylindrical excitation volume with a diameter of 600 μm and length of 1000 μm. The microwave field is generated by an Analog Signal Generator (Keysigh N5183B), which is calibrated with an SRS Model FS725 Rubidium clock oscillator, and emitted by a horn antenna with a frequency range of 22-33 GHz. A pair of electrode plates along the x-axis with a hollow in the center is used to apply an electric field for ionizing the Rydberg atoms. Due to their different ionization limits for the laser-prepared nS and microwave-coupled nP Rydberg atoms, the arrival time of ionized signals on the microchannel plate (MCP) detector is different, allowing state-selective recording with a boxcar and data acquisition card. There are other two pairs of electrode plates (not shown in Fig. 1) placed on both sides of MOT in the y- and z-axis for applying the voltage to compensate the stray electric field. The stray electric field is less than 2 mV/cm after compensation. Furthermore, three pairs of Helmholtz coils are placed on either side of the MOT chamber, which is used to compensate the stray magnetic field and apply the weak magnetic field for investigating the Zeeman splittings. The stray magnetic field is less than 5 mG after magnetic field compensation.

An experimental timing sequence is plotted at the bottom of Fig. 1(b). The ground-state atoms are trapped in the center of the MOT at a temperature ~ 100 μK. After switching off the MOT beams 1 ms, two excitation lasers with a duration of 500 ns are applied for the preparation of the $nS_{1/2}$ Rydberg state. Rydberg atomic density is $3 \times 10^7 cm^{-3}$ and corresponding the atomic separation 24 μm, which yields an energy shift less than 10 Hz, having a negligible effect. Subsequently, 20 μs microwave pulse couples the neighboring Rydberg state $nS_{1/2} \rightarrow nP_J$, forming the microwave spectroscopy of Rydberg atoms. Finally, a ramped field is applied for field ionization of Rydberg atoms and detection with MCP.

3. Results and discussions

3.1. Microwave spectroscopy

In Fig. 2, we display microwave spectroscopy with microwave field coupling the Rydberg transition of $51S_{1/2} \rightarrow 51P_{1/2}$ for the microwave duration of 20 μs and frequency step of 2 kHz. Zero detuning displays the center-of-gravity of $51S_{1/2} \rightarrow 51P_{1/2}$ transition, related microwave frequency $f = 28.679$ GHz. We can clearly see two peaks in the spectrum, which are attributed to the hyperfine structure transition of $51S_{1/2}(F = 4) \rightarrow 51P_{1/2}(F' = 3)$ and $(F' = 4)$, respectively. Solid curves indicate the results of Lorentz fittings. The peak centers marked with two vertical dashed lines are extracted from fitting and the center frequencies are $x_c(F' = 3) = -81.08 \pm 0.79$ kHz and $x_c(F' = 4) = 62.92 \pm 0.70$ kHz, respectively. The splitting interval is 143.99 ± 1.05 kHz.

As we know that the hyperfine energy shift is described as [1,15,31,32],

$$\Delta E_{\mathrm{HFS}} = \frac{A_{\mathrm{HFS}}}{(n-\delta(n))^3}\mathbf{I}\cdot\mathbf{J} + \frac{B_{\mathrm{HFS}}}{(n\delta(n))^3}\frac{3(\mathbf{I}\cdot\mathbf{J})^2 + \frac{3}{2}(\mathbf{I}\cdot\mathbf{J}) - I(I+1)J(J+1)}{2I(2I-1)J(2J-1)}, \tag{1}$$

where $\delta(n)$ is the quantum defect of the Rydberg state, A_{HFS} is the magnetic dipole constant describing the nucleus and Rydberg electron interaction, B_{HFS} is the electric quadrupole constant that is equal to 0 for $nP_{1/2}$ [32], and C_{HFS} (not shown here) is the magnetic octupole constant.

The hyperfine structure derives from the Fermi contact interaction between the Rydberg electron and the nucleus which presents a positive correlation to the probability density of the Rydberg electron in the nucleus. Considering the short-range interaction scale $(n-\delta(n))^{-3}$ [10],

Optics EXPRESS

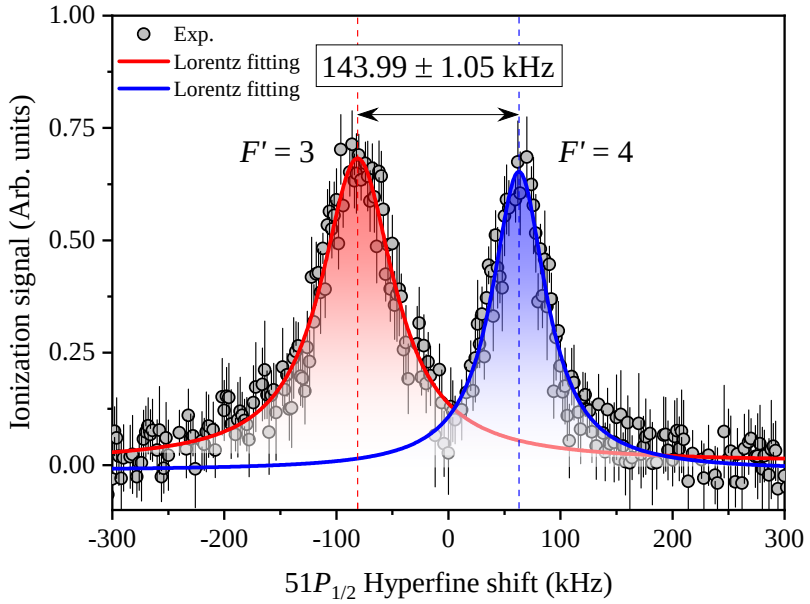

Fig. 2. Measured microwave spectrum of $51S_{1/2} \rightarrow 51P_{1/2}$ transition. Two peaks marked with vertical dashed lines are attributed to the hyperfine structure of $51P_{1/2}$ F'=3 and 4, corresponding to the center frequencies of $x_c(F' = 3) = -81.08 \pm 0.79$ kHz and $x_c(F' = 4) = 62.92 \pm 0.70$ kHz, respectively. The splitting interval is 143.99 ± 1.05 kHz. The linewidth (FWHM) is 79.17 ± 3.44 kHz and 59.13 ± 3.13 kHz, respectively. The solid lines are Lorenz fitting to the spectrum. Error bars come from the standard error mean (SEM) of 40 measurements.

the splitting interval can be written as [1,33],

$$\nu_{\mathrm{HFS}} = \frac{4A_{\mathrm{HFS}}}{(n-\delta(n))^3}\,. \tag{2}$$

For low lying 6P state, the hyperfine splitting is about a few hundred MHz, it is very easy to distinguish the hyperfine structure with the high-resolution spectroscopy such as saturated absorption spectroscopy. But for the Rydberg state, it is hard to resolve the hyperfine structure due to the Rydberg level space scaling n^{-3}. However, microwave spectroscopy of the Rydberg state with narrow linewidth allows us to investigate and distinguish the hyperfine structure splittings of the Rydberg state, as shown in Fig. 2. According to Eq. (2), we use the $nP_{1/2}$ quantum defect of δ_0=3.5915871(3), δ_2=0.36273(16) listed in Ref. [34] and the splitting interval of 143.99 ± 1.05 kHz in Fig. 2 to obtain the hyperfine structure constant of $A_{\mathrm{HFS}} = 3.84 \pm 0.03$ GHz, which is consist with the previous measurement [33].

Except for the hyperfine structure of Rydberg state $51P_{1/2}$ from the spectral profile, we also obtain the linewidth of full width at half maximum (FWHM) of 79.17 ± 3.44 kHz and 59.13 ± 3.13 kHz for $F' = 3$ and $F' = 4$, respectively. The linewidth is closer to the Fourier limit, which is 50 kHz for the microwave duration of 20 μs in this work but does not show a Fourier sideband like a sinc-like line shape which is because of the small effective Rabi frequency and large excitation laser detuning of $\delta_{852} = 2\pi \times 330$ MHz, seeing Ref. [35] for detailed. The lifetime-limited atomic linewidth of 2.97 kHz induced by spontaneous decay, which is far less than the Fourier limit, has a neglected effect. The experimental measured spectral linewidth is slightly larger than the Fourier limit, which may be attributed to the following reasons:

Optics EXPRESS

i) The uncertainty $\pm 5 \times 10^{-11}$ of microwave generator arises a negligible frequency shift of less than 10 Hz.

ii) Stark shift due to the stray electric field. Rydberg atom has large polarizability scaling as $\sim n^7$, therefore the weak stray field will lead to line broadening and shift. During the experiment, we apply an external DC-field in the three pairs of grids (only show one pair in Fig. 1(b)) to compensate the stray electric field by measuring the Stark shifts and splitting time to time, the details of electric field compensation see our previous work [11]. The final stray electric field is less than 2 mV/cm after compensation. According to the scalar polarizability of both Rydberg states, producing a frequency shift of 2 kHz, which is much less than the Fourier limit linewidth.

iii) Shift due to Rydberg-atom interactions. The calculation of Van del Waals dispersion coefficient of $|C_6| \approx 13.94$ GHz μm^6 and $|C_6| \approx 1.83$ GHz μm^6 for $51S_{1/2}$ and $51P_{1/2}$, respectively, causing a level shifts at 46 μm internuclear separation amount to only 2 Hz and are negligible.

iv) Zeeman shifts due to residual stray magnetic fields. In the presence of a weak magnetic field, the degeneration of Zeeman levels will be lifted due to the Zeeman effect, which results in three transition channels of $\Delta m_j = 0, \pm 1$, having a minor different transition frequency. After careful compensation of the magnetic field, there is still a weak residual magnetic field due to the material of the experimental device and environments, it is less than 5 mG in this work [36]. The line broadening due to the Zeeman shift can be written as $\Delta E_{|F,m_F\rangle} = \mu_B g_F m_F B_z$, here g_F is the Landé g-factor, calculated with $g_F \simeq g_J \frac{F(F+1)-I(I+1)+J(J+1)}{2F(F+1)}$. For example, a 4 mG stray magnetic field will cause a line broadening of 15 kHz for $50S_{1/2} \rightarrow 51P_{1/2}$ transition.

In addition, we use short excited laser pulse and small Rabi frequency of excitation lasers, the line shift and broadening due to Rydberg interaction is a few kHz that can be neglected. Therefore, the residual stray magnetic field is the main reason causing the line broadening of microwave spectroscopy that makes the spectral linewidth slightly larger than the Fourier limit. We investigate the Zeeman shift and splitting in the presence of the magnetic field in the next section.

3.2. Zeeman splittings spectroscopy

Zeeman effect is of great significance to understanding the structure of atomic and molecular energy levels and interaction between atoms and electromagnetic fields. For observing the spectral variations in the magnetic field, we record the microwave spectra of $51S_{1/2} \rightarrow 51P_J$ transition in the presence of a weak magnetic field that is along with the z direction. In Fig. 3, we present the measured microwave spectra with and without magnetic field. We can find that: i) in the absence of magnetic field ($B = 0$ mG), microwave spectrum of $51S_{1/2} \rightarrow 51P_{1/2}$ in Fig. 3(a1) shows two-peaks profile, which is attributed to the microwave coupled hyperfine transitions of $51S_{1/2}, F = 4 \rightarrow 51P_{1/2}, F' = 3$ and $F' = 4$, as mentioned before. But for $51S_{1/2} \rightarrow 51P_{3/2}$ transition in Fig. 3(b1), the microwave spectrum displays the broadened and asymmetric spectral profile, the hyperfine splittings are not clearly distinguished due to its small hyperfine splittings that is less than our spectral linewidth; ii) in the presence of the weak magnetic field, the microwave spectra both for $51S_{1/2} \rightarrow 51P_{1/2}$ in Fig. 3(a2), and $51S_{1/2} \rightarrow 51P_{3/2}$ transitions in Fig. 3(b2), display Zeeman level shifts and splittings. Compared with the microwave spectra without magnetic field, the spectra with the magnetic field split at least five peaks with frequency shifts, as shown in Fig. 3(b2) with B=100 mG. The Savitzky-Golay filtering method is used to smooth the spectrum, as shown with the red curve of Fig. 3.

Optics EXPRESS

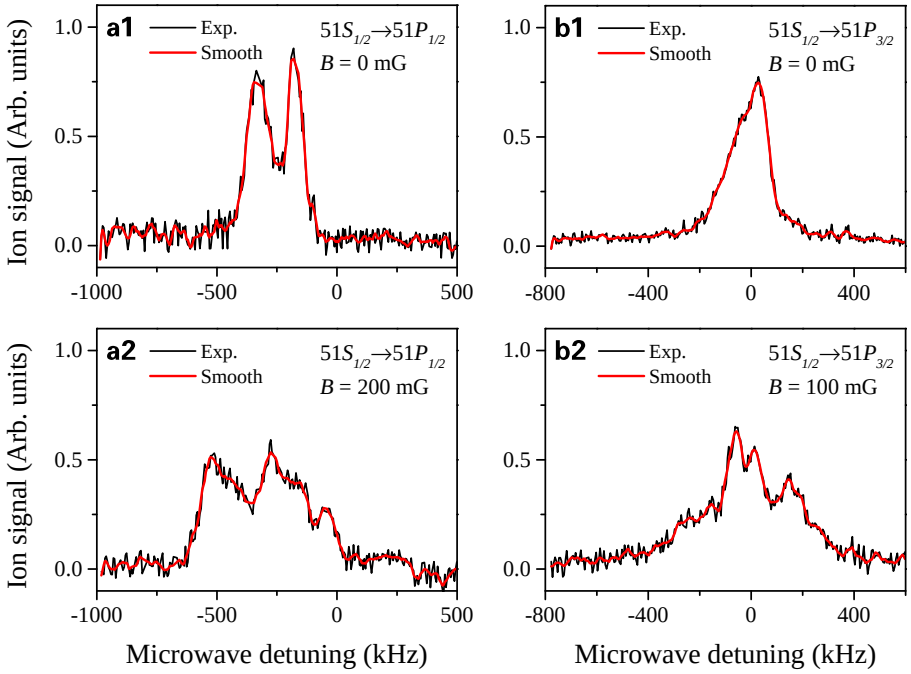

Fig. 3. Measured microwave spectra of $51S_{1/2} \rightarrow 51P_{1/2}$ transition (a) and $51S_{1/2} \rightarrow 51P_{3/2}$ transition (b) without (a1, b1) and with (a2, b2) a magnetic field. Red solid curves are the 19-smooth results with the Savitzky-Golay function.

To better understand the Zeeman spectroscopy and investigate the spectral evolution of the hyperfine structure for nP_J in the magnetic field, we first calculate Zeeman shifts and splittings of $51S_{1/2}$ and $51P_J$ states. The Hamiltonian of Rydberg state is written as $H = H_{HFS} + H_B$, here H_{HFS} is the HFS interaction and H_B is the Zeeman interaction for a magnetic field B being parallel

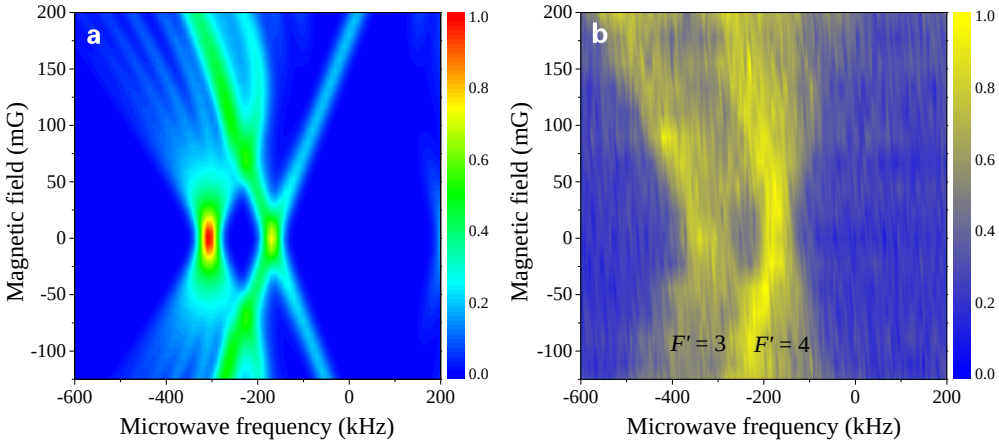

Fig. 4. Calculations (a) and measurements (b) of the Zeeman splitting of the $51S_{1/2}(F = 4) \rightarrow 51P_{1/2}(F' = 3, 4)$ hyperfine transitions, respectively. The applied magnetic field is parallel (in the z direction) to the microwave polarization. The color bar shows the normalized strength of the ion signal.

Optics EXPRESS

to the incident linear polarized microwave field. We diagonalize the Hamiltonian H and calculate the line strength by calculating the electric-dipole matrix elements between the eigenstates of H in the presence of the magnetic field. The details of the theoretical method see [1,37]. In Fig. 4(a), we present the simulated Zeeman splitting spectroscopy in linear color scale, which represents the signal strength of the microwave spectroscopy of $51S_{1/2}, (F = 4) \rightarrow 51P_{1/2}, (F' = 3, 4)$ transitions as the function of magnetic field and microwave frequency. It can be seen that at zero magnetic fields, the signal is strongest and decreases with the magnetic field. Meanwhile, the spectral lines are shifted and split into a few Zeeman lines with the intensity gradually decreasing. It is interesting to note that the spectra display the normal Zeeman effect when the magnetic field strength B <50 mG, where the spin-orbit interaction dominates over the effect of magnetic field, and hyperfine structure splitting between $F' = 3$ and $F' = 4$ linear increases with magnetic field, Zeeman splitting is larger than Zeeman shifts. The Zeeman lines of the $F' = 3$ and $F' = 4$ show a mixture when $B = 50$ mG. When the magnetic field strength increases further and larger than 50 mG, the spectra get into the strong field Paschen-Back regime, where the splitting and shift due to the magnetic field are larger than hyperfine splitting.

In the experiments, we change the currents of Helmholtz coils in z-axis to vary the magnetic field and make a series of measurements of microwave spectra for observing the hyperfine level splitting and shift in the weak magnetic field. In Fig. 4(b) we present the contour plot of the spectra as a function of microwave frequency and the strength of magnetic field, which shows an agreement with the simulations of Fig. 4(a). Close inspection of Fig. 4, we found that the field free line strength for $F' = 3$ is stronger than for $F' = 4$ in calculation, which shows a minor difference compared to the measurement. The difference in the field free line strength between the calculations and measurements can be attributed to the microwave polarization that might be varied at the MOT center due to our metal chamber.

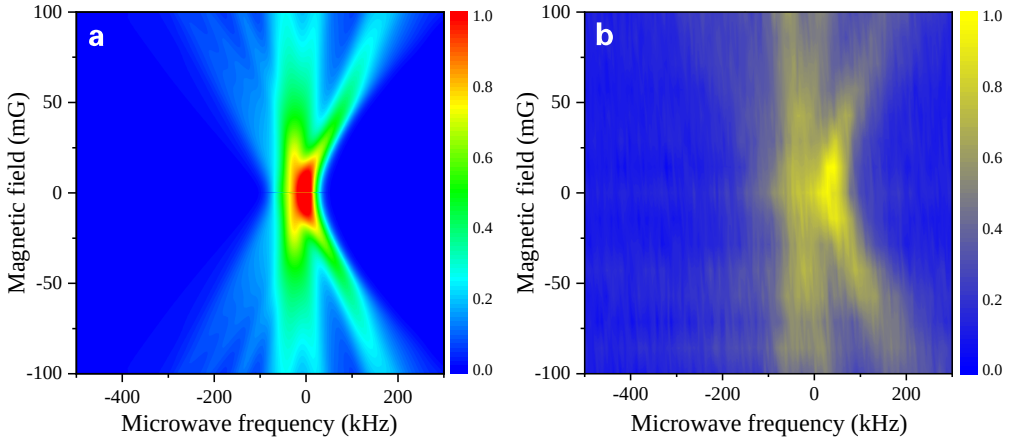

Fig. 5. Calculations (a) and experiments (b) of the Zeeman splittings of the $51S_{1/2}(F = 4) \rightarrow 51P_{3/2}$ transition. Due to the weak orbital and spin coupling of the Rydberg electron, the magnetic field-induced shifts and splitting are larger than the hyperfine structure splittings, the Zeeman spectroscopy for $51S_{1/2}(F = 4) \rightarrow 51P_{3/2}$ transition is being the strong Paschen-Back regime. The applied magnetic field is parallel (in the z direction) to the microwave polarization. The signal strength in calculations is displayed using a logarithm color scale to display the weak lines of the left sides clearly. It is seen that the measurements in (b) of the Zeeman splitting spectra show a good agreement with theoretical simulations in (a). The color bar shows the normalized strength of the ion signal.

In order to verify our theory, we do more simulations and measurements with microwave field coupling the $51S_{1/2} \rightarrow 51P_{3/2}$ transition, as shown in Fig. 5(a) for simulations and (b) for

Optics EXPRESS

experimental measurements. It is clearly seen that the experimental measurements show nice agreement with the simulations. Compared with the Zeeman spectra of the $51S_{1/2} \rightarrow 51P_{1/2}$ transition in Fig. 4, the Zeeman spectroscopy of the $51S_{1/2} \rightarrow 51P_{3/2}$ transition is in the strong field Paschen-Back regime and there is no normal Zeeman effect regime, as the hyperfine structure splitting is smaller than the Zeeman splitting, where the magnetic field is sufficiently strong to disrupt the coupling between orbital and spin angular momenta.

It can be seen from the above that the Zeeman splitting spectrum of the high lying Rydberg state within the weak magnetic field can be obtained using the narrow linewidth microwave spectroscopy. The Zeeman map displays different spectral profiles and characteristics for $51P_{1/2}$ and $51P_{3/2}$, which can be used to calibrate the magnetic field in the MOT center that can not be measured with normal magnetic field sensor. From the simulation, the different angles between the microwave polarization and magnetic field also lead to different spectral characteristics, which is used to analyze precisely magnetic field distribution.

4. Conclusion

In summary, we have investigated the hyperfine structure of $51P_{1/2}$ and Zeeman splitting spectra of the $51P_{1/2} \rightarrow 51P_J(J = 1/2, 3/2)$ Rydberg transition in an ultracold cesium atomic ensemble utilizing high-precise microwave spectroscopy. From the microwave spectra of $51S_{1/2}(F = 4) \rightarrow 51P_{1/2}$ transition, we resolved the hyperfine structure of $51P_{1/2}(F' = 3, 4)$ and obtained the hyperfine coupling constant of $A_{\mathrm{HFS}} = 3.84 \pm 0.03$ GHz. In addition, we have measured the Zeeman splitting spectra generated by hyperfine levels in the presence of a weak magnetic field, which is consistent with the theoretical simulation well. The weak field Zeeman spectra and strong field Paschen-Back effect of the Rydberg state help us to better understand the atomic and molecular level structure and to verify the theoretical model. The narrow linewidth microwave spectroscopy paves the way to precisely measure the magnetic field that can not be accessible with the usual magnetic sensor. Moreover, because of its polarization characteristics, the Zeeman effect plays an important role in applications such as medical imaging and astronomy.

Funding. National Natural Science Foundation of China (12120101004, 12241408, 62175136, U2341211); Fundamental Research Program of Shanxi Province (202303021224007); Scientific Cooperation Exchanges Project of Shanxi province (202104041101015); Program for Changjiang Scholars and Innovative Research Team in University (IRT 17R70); 1331 project of Shanxi province.

Acknowledgments. We thank Prof. Georg Raithel for his helpful discussion about calculations.

Disclosures. The authors declare no conflicts of interest related to this article.

Data availability. Data underlying the results presented in this paper are not publicly available at this time but may be obtained from the authors upon reasonable request.

References

1. R. Cardman and G. Raithel, "Hyperfine structure of $nP_{1/2}$ Rydberg states in ^{85}Rb," Phys. Rev. A **106**(5), 052810 (2022).
2. B. K. Teo, D. Feldbaum, T. Cubel, *et al.*, "Autler-townes spectroscopy of the $5S_{1/2} - 5p_{3/2} - 44d$ cascade of cold ^{85}Rb atoms," Phys. Rev. A **68**(5), 053407 (2003).
3. J. Bai, Y. Jiao, Y. He, *et al.*, "Autler-townes splitting of three-photon excitation of cesium cold Rydberg gases," Opt. Express **30**(10), 16748–16757 (2022).
4. G. R. Welch, M. M. Kash, C.-h. Iu, *et al.*, "Positive-energy structure of the diamagnetic Rydberg spectrum," Phys. Rev. Lett. **62**(17), 1975–1978 (1989).
5. R. V. Jensen, H. Flores-Rueda, J. D. Wright, *et al.*, "Structure of the stark recurrence spectrum," Phys. Rev. A **62**(5), 053410 (2000).
6. F. Engel, T. Dieterle, F. Hummel, *et al.*, "Precision spectroscopy of negative-ion resonances in ultralong-range Rydberg molecules," Phys. Rev. Lett. **123**(7), 073003 (2019).
7. S. Bai, X. Han, J. Bai, *et al.*, "Cesium $nD_J + 6S_{1/2}$ Rydberg molecules and their permanent electric dipole moments," Phys. Rev. Res. **2**(3), 033525 (2020).
8. F. Merkt and A. Osterwalder, "Millimetre wave spectroscopy of high Rydberg states," Int. Rev. Phys. Chem. **21**(3), 385–403 (2002).

Optics EXPRESS

9. Z. Bai, C. S. Adams, G. Huang, *et al.*, "Self-induced transparency in warm and strongly interacting Rydberg gases," Phys. Rev. Lett. **125**(26), 263605 (2020).
10. T. F. Gallagher, *Rydberg Atoms*, Cambridge Monographs on Atomic, Molecular and Chemical Physics (Cambridge University, 1994).
11. J. Bai, S. Bai, X. Han, *et al.*, "Precise measurements of polarizabilities of cesium *ns* Rydberg states in an ultra-cold atomic ensemble," New J. Phys. **22**(9), 093032 (2020).
12. M. S. O'Sullivan and B. P. Stoicheff, "Doppler-free two-photon absorption spectrum of cesium," Can. J. Phys. **61**(6), 940–948 (1983).
13. K. H. Weber and C. J. Sansonetti, "Accurate energies of *ns*, *np*, *nd*, *nf*, and *ng* levels of neutral cesium," Phys. Rev. A **35**(11), 4650–4660 (1987).
14. C. J. Lorenzen and K. Niemax, "Precise quantum defects of *ns*, *np* and *nd* levels in Cs I," Z Physik A **315**(2), 127–133 (1984).
15. E. Arimondo, M. Inguscio, and P. Violino, "Experimental determinations of the hyperfine structure in the alkali atoms," Rev. Mod. Phys. **49**(1), 31–75 (1977).
16. P. Goy, J. M. Raimond, G. Vitrant, *et al.*, "Millimeter-wave spectroscopy in cesium Rydberg states. quantum defects, fine- and hyperfine-structure measurements," Phys. Rev. A **26**(5), 2733–2742 (1982).
17. G. zu Putlitz and K. V. Venkataramu, "Hyperfeinstruktur und Lebensdauer des $8^2p_{3/2}$-Terms von Rubidium," Zeitschrift für Physik A Hadrons and nuclei **209**(5), 470–473 (1968).
18. W. Li, I. Mourachko, M. W. Noel, *et al.*, "Millimeter-wave spectroscopy of cold Rb Rydberg atoms in a magneto-optical trap: Quantum defects of the *ns*, *np*, and *nd* series," Phys. Rev. A **67**(5), 052502 (2003).
19. H. Saßmannshausen, F. Merkt, and J. Deiglmayr, "High-resolution spectroscopy of Rydberg states in an ultracold cesium gas," Phys. Rev. A **87**(3), 032519 (2013).
20. L. Zhang, S. Bao, H. Zhang, *et al.*, "Interplay between optical pumping and Rydberg eit in magnetic fields," Opt. Express **26**(23), 29931–29944 (2018).
21. S. Bao, H. Zhang, J. Zhou, *et al.*, "Polarization spectra of Zeeman sublevels in Rydberg electromagnetically induced transparency," Phys. Rev. A **94**(4), 043822 (2016).
22. H. Cheng, H. M. Wang, S. S. Zhang, *et al.*, "High resolution electromagnetically induced transparency spectroscopy of Rydberg ^{87}Rb atom in a magnetic field," Opt. Express **25**(26), 33575–33587 (2017).
23. Y. Xue, L. Hao, Y. Jiao, *et al.*, "Rydberg electromagnetically induced transparency in a large hilbert space," Phys. Rev. A **99**(5), 053426 (2019).
24. F. Jia, Y. Yu, X. Liu, *et al.*, "Dispersive microwave electrometry using Zeeman frequency modulation spectroscopy of electromagnetically induced transparency in Rydberg atoms," Appl. Opt. **59**(27), 8253–8258 (2020).
25. F. Jia, J. Zhang, L. Zhang, *et al.*, "Frequency stabilization method for transition to a Rydberg state using Zeeman modulation," Appl. Opt. **59**(7), 2108–2113 (2020).
26. E. Urban, T. A. Johnson, T. Henage, *et al.*, "Observation of Rydberg blockade between two atoms," Nat. Phys. **5**(2), 110–114 (2009).
27. F. Böttcher, A. Gaj, K. M. Westphal, *et al.*, "Observation of mixed singlet-triplet Rb_2 Rydberg molecules," Phys. Rev. A **93**(3), 032512 (2016).
28. L. Ma, D. A. Anderson, and G. Raithel, "Paschen-back effects and Rydberg-state diamagnetism in vapor-cell electromagnetically induced transparency," Phys. Rev. A **95**(6), 061804 (2017).
29. X. Li, Y. Cui, J. Hao, *et al.*, "Magnetic-field-induced splitting of Rydberg electromagnetically induced transparency and autler-townes spectra in ^{87}Rb vapor cell," Opt. Express **31**(23), 38165–38178 (2023).
30. Y. Shi, C. Li, K. Ouyang, *et al.*, "Tunable frequency of a microwave mixed receiver based on Rydberg atoms under the Zeeman effect," Opt. Express **31**(22), 36255–36262 (2023).
31. A. Corney, *Atomic and Laser Spectroscopy* (Oxford University, 2006).
32. D. A. Steck, "Cesium D line data," https://steck.us/alkalidata/cesiumnumbers.pdf (2019).
33. M. Allegrini, E. Arimondo, and L. A. Orozco, "Survey of Hyperfine Structure Measurements in Alkali Atoms," J. Phys. Chem. Ref. Data **51**(4), 043102 (2022).
34. J. Deiglmayr, H. Herburger, H. Saßmannshausen, *et al.*, "Precision measurement of the ionization energy of Cs I," Phys. Rev. A **93**(1), 013424 (2016).
35. J. Bai, R. Song, Z. Li, *et al.*, "Microwave spectroscopy and Zeeman effect of cesium $(n+2)D_{5/2} \rightarrow nF_J$ Rydberg transitions," arXiv, arXiv 2309.04749 (2023).
36. J. Bai, R. Song, J. Fan, *et al.*, "Quantum defects of nF_J levels of Cs Rydberg atoms," Phys. Rev. A **108**(2), 022804 (2023).
37. A. Ramos, R. Cardman, and G. Raithel, "Measurement of the hyperfine coupling constant for $nS_{1/2}$ Rydberg states of ^{85}Rb," Phys. Rev. A **100**(6), 062515 (2019).